PHYSICAL REVIEW D **87,** 026005 (2013)

# Electromagnetic signature in holographic plasma with *B* field

Yanyan Bu*

*State Key Laboratory of Theoretical Physics, Institute of Theoretical Physics, Chinese Academy of Science, Beijing 100190, People's Republic of China, University of Chinese Academy of Sciences, Yuquan Road 19A, Beijing 100049, People's Republic of China, and Max-Planck-Institut für Physik (Werner-Heisenberg-Institut), Föhringer Ring 6, 80805 München, Germany*

(Received 15 October 2012; published 24 January 2013)

We explore the effect of a magnetic field on the electromagnetic signature in QCD-like plasma by taking the AdS/CFT approach. Concretely, we choose two QCD gravity dual models to do comparative studies: the D4/D6 and D3/D7 models. The magnetic field is simulated by a spatial component of the flavor U(1) gauge field in the bulk side. For both models, we plot the spectral function and photoemission rate for lightlike momenta as well as the ac conductivity. Due to the presence of the magnetic field, the rotational symmetry is partially broken. Therefore, we plot the spectral function and photoemission rate with spatial momentum parallel or perpendicular to the magnetic field, respectively. We find that the magnetic field induces an anisotropic feature in the electromagnetic signature. To be specific, when the emitted photons from the plasma are moving along the magnetic field, the electromagnetic signature is weakened as the magnetic field is increasing; on the contrary, when the produced photons move perpendicular to the magnetic field, the magnetic field has the effect of amplifying the electromagnetic signature. This should have a relationship with the anisotropic feature of the photon signal observed in heavy-ion collision experiments. This anisotropic characteristic can also be observed in the ac conductivity of the holographic plasma. In the infrared regime of the frequency, the magnetic field suppresses the ac conductivity (along the direction perpendicular to the magnetic field) and likely gives a pseudogap structure. However, the ac conductivity along the magnetic field is enhanced due to the presence of the magnetic field.

DOI: 10.1103/PhysRevD.87.026005 PACS numbers: 11.25.Tq

## I. INTRODUCTION

Data from relativistic heavy-ion collision (RHIC) experiments seem to indicate that the QCD plasma is strongly coupled and behaves like a perfect liquid [1]. This brings nonperturbative investigations of hadronic matter at high temperature and high density, produced in RHIC experiments, into an urgent stage. The lattice method, used to explore some properties of thermal QCD, is still constrained to extract static quantities of QCD of the strongly coupled regime, such as the hadron mass spectrum and thermodynamical behavior. Therefore, improvement in the theoretical understanding of strongly coupled quark-gluon plasma (sQGP) should not only go beyond the traditional perturbative QCD approach, but should also reveal some properties out of equilibrium, such as transport properties, dispersion relations, and high-energy scattering.

AdS/CFT correspondence [2], which is based on string/M-theory, is a powerful tool in investigating the strong coupling regime of non-Abelian gauge field theory and has given us some insight into properties of sQGP; see Ref. [3] for an incomplete list of recent reviews. What is more attractive is that this approach gives us an analytical treatment of the strong-coupling regime of gauge field theory. However, it is still a mystery why these calculations based on large-$N$ gauge theory—mostly $N = 4$ supersymmetric Yang-Mills (SYM) theory—can match so well with QCD phenomena. Actually, there are some attempts to construct a QCD gravity dual under the framework of gauge/gravity duality in the hope of mimicking the behavior of realistic QCD phenomena at low energy or QCD plasma; see Refs. [4–6] for original references.

Photon or dilepton production—which should be an important signal of sQGP and which carries some key information of sQGP in the early stage—in $N = 4$ SYM plasma were discussed in detail both in the strong-and weak-coupling regime in Ref. [7]. It was found there that the current-current spectral functions in the strongly coupled theory exhibit hydrodynamic peaks at small frequencies, but otherwise show no peak structure which could be interpreted as well-defined thermal resonances in the high-temperature phase. Following this pioneering work, the analysis was soon generalized to D3/D7 and D4/D6 brane systems in Ref. [8], a high-temperature version of the Sakai-Sugimoto model in Ref. [9], the soft-wall AdS/QCD model in Ref. [10], the strongly coupled anisotropic plasma in Ref. [11], and the $N = 4$ SYM plasma at large but finite 't Hooft coupling in Ref. [12]. Some references [9,13–15] also studied the photoemission rate at finite charge density by taking the AdS/CFT correspondence. All of these works have seen some common features of photoproduction from QCD-like plasma, which indicates that AdS/CFT correspondence can be thought of as a useful tool in describing universal properties of the strong-coupling

*yybu@itp.ac.cn

 

regime of QCD plasma. The results in Refs. [15–18] seem to indicate that the internal space in critical supergravity has no essential effect on the physical results that concern us. Therefore, in this work we take the D4/D6 and D3/D7 models, which are the most studied holographic models under the top-down approach, to carry out our computations.

On the other hand, the effects of external magnetic fields on strongly coupled dynamics in the context of the AdS/CFT correspondence has proved to be an enormously fruitful area of study. Within the area of probe D-brane physics, the phenomenology of an external magnetic field was first studied in Ref. [19] by taking the D3/D7 model, where it was shown that the magnetic field could be used to induce a chiral-symmetry-breaking phase transition while giving Zeeman splitting. In Refs. [20,21] this was studied at finite temperature and it was shown that the magnetic field would act to stabilize the meson, which would otherwise melt into the quark-gluon plasma.

Coming back to the sQGP produced in the RHIC experiments, the photoproduction plays an important role in unraveling the properties of hot and dense matter. However, recent measurements by the PHENIX collaboration [22] revealed that the anisotropy of produced photons is very close to that of hadrons. This thus raises a new challenge for the theoretical description of properties of heavy-ion collisions. One proposal [23] for the anisotropic feature of the photon signal is based on the presence of a large magnetic field in heavy-ion collisions. Actually, it was already recognized in Ref. [24] that the magnetic field plays an important role in the understanding of heavy-ion collisions.

Motivated by these studies and the results mentioned above, in this paper we probe the effect of a magnetic field from the flavor sector on the photoproduction rate and ac conductivity of the dual plasma; to be specific, the D3/D7 and D4/D6 brane models. For the photoemission, we find that both models give similar results, which is consistent with previous studies. Due to the presence of the magnetic field, the spatial rotational symmetry is partially broken to SO(2), i.e., rotation in the plane perpendicular to the magnetic field. Explicitly, the anisotropic feature sets in: it is reasonable to expect that the produced photons should behave differently according to their spatial momentum with respect to the direction of the magnetic field. Our findings are that when the magnetic field is parallel to the spatial momentum of the produced photons the magnetic field weakens the electromagnetic signature; in sharp contrast to this, when they are orthogonal to each other, the magnetic field has the effect of amplifying the electromagnetic signature. We also plotted the ac conductivity of the dual plasma. In the infrared regime of the frequency, the magnetic field makes the ac conductivity (along the direction perpendicular to the magnetic field) become suppressed, likely giving a pseudogap structure. However, the ac conductivity along the magnetic field is enhanced due to the presence of the magnetic field.

The rest of this paper is organized as follows. In Sec. II we concisely introduce our holographic setup and then review the computations of the photon production rate and conductivity using the AdS/CFT approach, which can be found in Ref. [7]. Sections III and IV are devoted to numerical computations of the photoproduction rate and plasma conductivity in all regimes of the frequency for both models. We summarize our work in Sec. V.

## II. HOLOGRAPHIC SETUP AND PHOTOPRODUCTION IN THERMAL FIELD THEORY

### A. Formulas for photoproduction and plasma conductivity

Spontaneous photoproduction from a medium that is composed of electrically charged particles is a good signal to probe its properties. The spectra of produced photons depend on the details of the system. Moreover, it is expected that the emitted photon from a quark-gluon plasma (QGP) has little to do with the black-body radiation distribution, but it may give valuable information about the properties of the QGP. However, as mentioned at the beginning of Sec. I, the produced QGP in RHIC experiments is perhaps strongly coupled and we therefore need a nonperturbative treatment of the calculations of the photoemission from the sQGP. This is why AdS/CFT correspondence sets in and plays a more and more important part in studying the properties of sQGP. We here follow Ref. [7] to briefly list basic formulas for computing the photoproduction rate and ac conductivity associated with QCD-like plasma.

Consider a thermal system, which can be described by finite-temperature quantum field theory. We assume that the interaction between the photon and matter takes the electromagnetic current form $eJ_\mu A^\mu$, where $J_\mu$ is the electromagnetic current and $e$ is the electromagnetic coupling constant. From thermal field theory [25], the photoproduction rate $\Gamma_\gamma$ from a thermal system in equilibrium, to leading order in $e$, is given by

$$d\Gamma_\gamma = \frac{d^3q}{(2\pi)^3 2\omega} e^2 n_B(\omega)\eta^{\mu\nu}\chi_{\mu\nu}(k)|_{\omega=|\vec{q}|}, \tag{1}$$

where $n_B = 1/(e^{\omega/T}-1)$ is the Bose-Einstein distribution function, $k^\mu = (\omega, \vec{q})$ is the four-momentum vector, $\eta_{\mu\nu} = (-1, 0, 0, 0)$ denotes the Minkowski metric, and $\chi_{\mu\nu}$ is the spectral function, defined by the following equations:

$$\begin{aligned} \chi_{\mu\nu}(k) &= -2\mathrm{Im}G^R_{\mu\nu}(k), \\ G^R_{\mu\nu}(k) &= \int d^4x e^{-ik\cdot x}\langle J_\mu(0)J_\nu(x)\rangle_T \theta(-t). \end{aligned} \tag{2}$$

Here, the symbol $\langle\cdots\rangle_T$ denotes the expectation value taken in the thermal equilibrium state, and $x^\mu = (t, \vec{x})$. The ac conductivity can be extracted from the Kubo formula,

$$\sigma(\omega) = \frac{G^R_{ii}(\omega, \vec{k} = 0)}{i\omega}, \tag{3}$$

where $G^R_{ii}(\omega, \vec{k} = 0)$ denotes the spatial component of the retarded Green's function $G^R_{\mu\nu}(\omega, \vec{k} = 0)$.

At nonzero temperature, the Lorentz invariance of relativistic quantum field theory is explicitly broken. Fortunately, the unbroken rotational symmetry and gauge invariance allow one to decompose the retarded Green's function $G^R_{\mu\nu}(k)$ into transversal and longitudinal parts [26] as follows:

$$G^R_{\mu\nu}(k) = P^T_{\mu\nu}(k)\Pi^T + P^L_{\mu\nu}(k)\Pi^L(k). \tag{4}$$

The projective operators are defined as

$$\begin{aligned} P^T_{ij}(k) &= \delta_{ij} - \frac{q_i q_j}{|\vec{q}|^2}, \qquad P^T_{0\nu} = 0, \\ P^L_{\mu\nu}(k) &= \eta_{\mu\nu} - \frac{k_\mu k_\nu}{k^2} - P^T_{\mu\nu}(k). \end{aligned} \tag{5}$$

Plugging the above operators into Eq. (4) results in the following form for the trace of the spectral function:

$$\chi^\mu_\mu = -4\mathrm{Im}\Pi^T(k) - 2\mathrm{Im}\Pi^L(k). \tag{6}$$

Recall that in this paper we focus on the real photon production and therefore set $\omega = |\vec{q}|$. Then, only the transversal part $\Pi^T(k)$ contributes to the trace of the spectral density (because if $\Pi^L(k) \neq 0$, there will be a singularity in the retarded Green's function due to the lightlike momenta chosen for the real photon production).

In summary, the goal of revealing the photoproduction and ac conductivity of the sQGP is reduced to calculations of the retarded Green's function for the electromagnetic current $J_\mu$. Under AdS/CFT correspondence, by weakly gauging the flavor U(1) symmetry in the world-volume of the probe D-brane and treating it as an analogue of the electromagnetic symmetry our task is further reduced to computing this flavor current-current correlator under the prescription given in Ref. [27].

### B. Holographic setup for the QCD gravity dual

In general, the QCD gravity dual can be summarized as the following geometric metric with one dilaton background $\phi$:

$$ds^2 = g_{tt}dt^2 + g_{uu}du^2 + g_{ij}dx^i dx^j + g_S dS^2, \tag{7}$$

where $dS^2$ denotes the internal space of ten-dimensional supergravity geometry. The above metric and dilaton can be sourced by the Einstein-dilaton system. To make the dual QCD-like theory at finite temperature, one can push the above geometry to a black hole and identify the Hawking temperature as that of the dual-boundary field theory. To mimic an external magnetic field, we take a probe D-brane method and turn on the background for the spatial component of the flavor U(1) gauge field, $A_x$. Here, we assume a constant magnetic field, i.e., $A_x = By$, with $B$ a constant. The embedding profile $\chi(u)$ of the probe D-brane can be determined by minimizing the Dirac-Born-Infeld (DBI) action for the probe D-brane. However, we here choose the trivial profile $\chi'(u) = 0$ to simplify our analysis and leave the complicated flavor embedding profile for a future publication.

With the above assumptions, the DBI action[1] for the probe Dq-brane is

$$S = -T_q N_f \int d^{q+1}x e^{-\phi}\sqrt{-\det(g + F^0)}, \tag{8}$$

where we set $2\pi l_s^2 = 1$ for brevity, $N_f$ denotes the number of flavor branes, $g$ is the induced metric in the flavor world-volume, and $F^0$ is the field strength constructed from $A_x$. We then fluctuate the system and compute the current-current correlator following the prescription of Ref. [27].

## III. D4/D6 MODEL

Since the seminal paper [28], intersecting D-brane systems have been widely used to study flavored large-$N$ gauge theory at strong coupling, in the hopes of giving some physical intuition to nonperturbative QCD. These investigations indeed have produced fruitful conclusions. In this section we also take the intersecting D-brane system as our starting point. To be specific, we choose the D4/D6 model as the QCD gravity dual. This model was first studied in Ref. [4] and revealed many interesting properties for hadron physics in QCD. It is based on the D4-brane geometry in type IIA supergravity,

$$\begin{aligned} ds^2 = &\left(\frac{u_0}{R}\right)^{3/2} u^{-3/2}(-f(u)dt^2 + d\vec{x}^2 + dx_4^2) \\ &+ R^{3/2}u_0^{1/2}u^{-5/2}\frac{du^2}{f(u)} + R^{3/2}u_0^{1/2}u^{-1/2}d\Omega_4^2 \end{aligned} \tag{9}$$

with the internal space $\Omega_4$ parametrized as

$$d\Omega_4^2 = d\theta^2 + \cos^2\theta d\Omega_2^2 + \sin^2\theta d\xi^2, \tag{10}$$

where the blackening factor is $f(u) = 1 - u^3$. There is also a background for the dilaton field $e^\phi = g_s(u_0/R)^{3/4}u^{-3/4}$. In our convention for the metric, the black hole horizon is located at $u = 1$, and $u = 0$ denotes the conformal boundary where the dual field theory lives. To avoid a conical singularity in the $(t, u)$ plane, the time direction should be periodically identified, i.e., $t \sim t + \beta$ with the Hawking temperature $T = 1/\beta = \frac{3}{4\pi}u_0^{1/2}/R^{3/2}$.

The flavor D6-brane extends along $(t, \vec{x}, u, \Omega_2)$ and its embedding profile is specified by $\theta(u)$. As mentioned in Sec. II, in this paper we choose the trivial profile for the flavor sector, i.e., $\theta(u) = 0$, and the induced metric on the flavor world-volume is as follows:

[1]We here focus on the U(1) part of the DBI action, and there is no Chern-Simons term in our case, which is due to the trivial embedding profile of the probe brane.

$$ds^2_{\rm ind} = \left(\frac{u_0}{R}\right)^{3/2} u^{-3/2}(-f(u)dt^2 + d\vec{x}^2) + R^{3/2}u_0^{1/2}u^{-5/2}\frac{du^2}{f(u)} + R^{3/2}u_0^{1/2}u^{-1/2}d\Omega_2^2. \quad (11)$$

To study the photoproduction signal, we need to perturb the system by including a fluctuation of gauge field, $A_M \to A_M + a_M$, where $M$ denotes all the indices in Eq. (11). To quadratic order in the gauge field fluctuation $a_M$, the DBI action can be expanded to the following form [we here omit the background part, as in Eq. (8)]:

$$S_{fl} = -\frac{N_f T_6}{4}\int d^4x du d\Omega_2 e^{-\phi}\sqrt{-\det(g_{\rm ind}+F^0)}f_{MN}f^{MN} \equiv -\frac{\mathcal{N}'}{4}\int dx^4 du\sqrt{-\mathcal{G}}f_{\mu\nu}f^{\mu\nu}. \quad (12)$$

In the second equality of above equation, we have assumed that the fluctuation $a$ is a singlet with respect to the internal space $\Omega_2$, and we have also chosen the components of $a$ along $\Omega_2$ to be zero and have absorbed the integration over $\Omega_2$ to the prefactor $\mathcal{N}'$. With the residual SO(2) rotational symmetry, we can take the Fourier ansatz for $a_\mu$ of the form

$$a_\mu(t,\vec{x},u) = \int \frac{d^4k}{(2\pi)^4}a_\mu(k,u;B)e^{-i\omega t+\vec{k}\cdot\vec{x}}, \quad \text{with} \quad \vec{k} = (q,0,0) \quad \text{or} \quad (0,0,q). \quad (13)$$

The contraction of indices $\mu$, $\nu$ uses the symmetric part $G$ of $(g_{\rm ind}+F^0)^{-1}$ defined as follows:

$$(g_{\rm ind}+F^0)^{-1} = G + J, \quad (14)$$

with the diagonal part of $G$ given by

$$G^{\mu\nu} = \mathrm{diag}\left(g^{tt}, \frac{g_{yy}}{g_{yy}g_{xx}+(\partial_y A_x)^2}, \frac{g_{xx}}{g_{yy}g_{xx}+(\partial_y A_x)^2}, g^{zz}, g^{uu}\right). \quad (15)$$

The equation of motion for the gauge field fluctuation $a_M$ is simply the Maxwell equation,

$$\partial_\mu\left(\sqrt{-\mathcal{G}}f^{\mu\nu}\right) = 0, \quad (16)$$

where $f_{\mu\nu} = \partial_\mu a_\nu - \partial_\nu a_\mu$ is the gauge field strength for the fluctuation part. In the presence of a magnetic field, we have to treat the system separately according to the direction of the spatial momentum $\vec{k}$: $\vec{k} \parallel B$ or $\vec{k} \perp B$.[2]

### A. The case $\vec{k} = (0, 0, q)$

We first explicitly write down the equations of motion for different modes. For the longitudinal modes $\{a_t(k,u;B), a_z(k,u;B)\}$, there are two second-order differential equations and one constraint coming from the gauge choice $a_u = 0$:

$$\begin{aligned}
&\partial_u^2 a_t(k,u;B) + \partial_u \ln\left(\sqrt{-\mathcal{G}}G^{uu}G^{tt}\right)\partial_u a_t(k,u;B) - \frac{G^{zz}}{G^{uu}}(q^2 a_t(k,u;B) + q\omega a_z(k,u;B)) = 0,\\
&\partial_u^2 a_z(k,u;B) + \partial_u \ln\left(\sqrt{-\mathcal{G}}G^{uu}G^{zz}\right)\partial_u a_z(k,u;B) - \frac{G^{tt}}{G^{uu}}(\omega^2 a_z(k,u;B) + q\omega a_t(k,u;B)) = 0,\\
&\omega G^{tt}\partial_u a_t(k,u;B) - qG^{zz}\partial_u a_z(k,u;B) = 0.
\end{aligned} \quad (17)$$

As usual, one can define one gauge-invariant mode to decouple the two modes in Eq. (17),

$$E = \omega a_z(k,u;B) + q a_t(k,u;B),$$

which obeys the equation of motion as follows:

$$\partial_u^2 E + \left[\frac{f'(u)}{f(u)} - \frac{g'(u)}{2g(u)} + \frac{\tilde{q}^2 f'(u)}{\tilde{\omega}^2 - \tilde{q}^2 f(u)}\right]\partial_u E + \left(\frac{\tilde{\omega}^2}{uf(u)^2} - \frac{\tilde{q}^2}{uf(u)}\right)E = 0, \quad (18)$$

with the dimensionless frequency and momentum defined as

$$\tilde{\omega} = \frac{3}{4\pi T}\omega, \qquad \tilde{q} = \frac{3}{4\pi T}q, \quad (19)$$

and the function $g(u)$ given by

$$g(u) = 1 + \tilde{B}^2 u^3, \qquad \tilde{B} = \left(\frac{R}{u_0}\right)^{3/2}B. \quad (20)$$

Explicitly, this mode also feels the effect of the magnetic field. However, it has no contribution to the spectral function for the photon signal $\tilde{\omega} = \tilde{q}$. This can be easily understood by taking the limit case $B \to 0$ and requiring that the results go back to the previous conclusion that the longitudinal modes have no contribution to the photoemission rate. We have checked this conclusion by numerically computing the retarded Green's function for the $E$ mode when setting the lightlike momentum $\tilde{\omega} = \tilde{q}$ and found that it is zero. We therefore do not consider this mode further.

We now turn to the transverse modes $\{a_x(k,u;B), a_y(k,u;B)\}$. They both obey the same equation of motion and so we take the $a_y(k,u;B)$ mode as the example:

$$\partial_u^2 a_y(k,u;B) + \partial_u \ln\left(\sqrt{-\mathcal{G}}G^{uu}G^{yy}\right)\partial_u a_y(k,u;B) - \left(\frac{G^{tt}}{G^{uu}}\omega^2 + \frac{G^{zz}}{G^{uu}}q^2\right)a_y(k,u;B) = 0. \quad (21)$$

[2]We do not consider the general case where all three components of the spatial momentum are nonzero by simplifying our analysis.

As in the longitudinal modes, in deriving this equation the radial gauge $a_u = 0$ has been chosen. By substituting the metric in Eq. (15) into Eq. (21) and simplifying by some algebraic manipulations, we obtain the following equation:

$$\partial_u^2 a_y(k,u;B) + \left[\frac{f'(u)}{f(u)} - \frac{g'(u)}{2g(u)}\right]\partial_u a_y(k,u;B) + \left[\frac{\tilde{\omega}^2}{uf(u)^2} - \frac{\tilde{q}^2}{uf(u)}\right]a_y(k,u;B) = 0. \tag{22}$$

In order to compute the retarded Green's function for the operator dual to the $a_y$ mode, we use the equation of motion as in Eq. (21) to change the action in Eq. (12) to the following form by integrating by parts:

$$S_{fl} = -\frac{\mathcal{N}'}{2}\int\frac{d^4k}{(2\pi)^4} \times \left\{\sqrt{-\mathcal{G}}G^{uu}G^{yy}a_y(-k,u;B)\partial_u a_y(k,u;B)\right\}\Big|_{u=0}^{u=1}. \tag{23}$$

Then, following the prescription of Ref. [27], the retarded Green's function for the mode $a_y$ is given by

$$G^R_{yy}(k) = \mathcal{N}'\frac{\sqrt{-\mathcal{G}}G^{uu}G^{yy}a_y(-k,u;B)\partial_u a_y(k,u;B)}{a_y(-k,0;B)a_y(k,0;B)}\Big|_{u=0}, \tag{24}$$

with $a_y(k,u;B)$ taking the ingoing-wave boundary condition at the horizon $u = 1$.

Generically, one cannot get an analytical solution to Eq. (22) in the whole regime of parameters $\{\tilde{\omega}, \tilde{q}, \tilde{B}\}$, so we therefore turn to solving it numerically. We begin by analyzing the asymptotic behaviors for $a_y(k,u;B)$ near the conformal boundary $u = 0$ and the horizon $u = 1$. Frobenius analysis reveals that, near the horizon $u = 1$,

$$a_y(k,u\sim 1;B) \simeq (1-u)^{-i\tilde{\omega}/3}[1 + a_y^{(1)}(1-u) + a_y^{(2)}(1-u)^2 + a_y^{(3)}(1-u)^3 + \cdots], \tag{25}$$

where we have set the scale of $a_y(k,u;B)$ to one by taking advantage of the linearity of Eq. (22), and the minus index $-i\tilde{\omega}/3$ is chosen for the ingoing-wave boundary condition at the horizon for the purpose of the retarded Green's function; near the conformal boundary $u = 0$,

$$a_y(k,u\sim 0;B) \simeq a_y(k,0;B) + u a_y^1(k,0;B) + \cdots \tag{26}$$

In Eq. (25), these expansion coefficients are uniquely determined in terms of the three parameters $\{\tilde{\omega}, \tilde{q}, \tilde{B}\}$. We take the expansion solution near the horizon in Eq. (25) as the initial conditions and use the MATHEMATICA command "NDSolve" to solve Eq. (22) numerically. The retarded Green's function can be easily read off from the expansion in Eq. (26) and the formula in Eq. (24):

$$G^R(k) = \mathcal{N}\frac{a_y^1(k,0;B)}{a_y(k,0;B)}. \tag{27}$$

Roughly speaking, the factor $\mathcal{N}$ counts the degrees of freedom for the flavor sector, $\mathcal{N}\sim N_f N_c$. The explicit form of the normalization factor $\mathcal{N}$ will be given at the end of Sec. IV.

### B. The case $\vec{k} = (q, 0, 0)$

This case is more complicated than the case in Sec. III A, as will be clear in the following. First consider the coupled modes, i.e., the longitudinal modes $\{a_t(k,u;B), a_x(k,u;B)\}$:

$$\begin{aligned}
&\partial_u^2 a_t(k,u;B) + \partial_u \ln\left(\sqrt{-\mathcal{G}}G^{uu}G^{tt}\right)\partial_u a_t(k,u;B) - \frac{G^{xx}}{G^{uu}}(q^2 a_t(k,u;B) + q\omega a_x(k,u;B)) = 0,\\
&\partial_u^2 a_x(k,u;B) + \partial_u \ln\left(\sqrt{-\mathcal{G}}G^{uu}G^{xx}\right)\partial_u a_x(k,u;B) - \frac{G^{tt}}{G^{uu}}(\omega^2 a_x(k,u;B) + q\omega a_t(k,u;B)) = 0,\\
&\omega G^{tt}\partial_u a_t(k,u;B) - qG^{xx}\partial_u a_x(k,u;B) = 0.
\end{aligned} \tag{28}$$

Following the same trick in Sec. III A, we can define a gauge-invariant mode to decouple these two modes, $E = \omega a_x(k,u;B) + q a_t(k,u;B)$, which satisfies the equation of motion

$$\partial_u^2 E + \left[\frac{f'(u)}{f(u)} - \frac{g'(u)}{2g(u)} + \frac{\tilde{q}^2\left(\frac{f(u)}{g(u)}\right)'}{\tilde{\omega}^2 - \tilde{q}^2\frac{f(u)}{g(u)}}\right]\partial_u E + \left(\frac{\tilde{\omega}^2}{uf(u)^2} - \frac{\tilde{q}^2}{uf(u)g(u)}\right)E = 0. \tag{29}$$

Similar to Eq. (18) in Sec. III A, this mode also feels the presence of the magnetic field. Fortunately, following the same arguments below Eq. (20), it still contributes nothing to the photoemission rate. We have numerically checked this conclusion.

Besides the longitudinal modes, the transverse modes also behave differently than those in Sec. III A; $a_y(k,u;B)$ and $a_z(k,u;B)$ have different equations of motion:

$$\partial_u^2 a_y(k,u;B) + \left[\frac{f'(u)}{f(u)} - \frac{g'(u)}{2g(u)}\right]\partial_u a_y(k,u;B) + \left[\frac{\tilde{\omega}^2}{uf(u)^2} - \frac{\tilde{q}^2}{uf(u)g(u)}\right]a_y(k,u;B) = 0, \tag{30}$$

$$\partial_u^2 a_z(k,u;B) + \left[\frac{f'(u)}{f(u)} + \frac{g'(u)}{2g(u)}\right]\partial_u a_z(k,u;B) + \left[\frac{\tilde{\omega}^2}{uf(u)^2} - \frac{\tilde{q}^2}{uf(u)g(u)}\right]a_z(k,u;B) = 0. \tag{31}$$

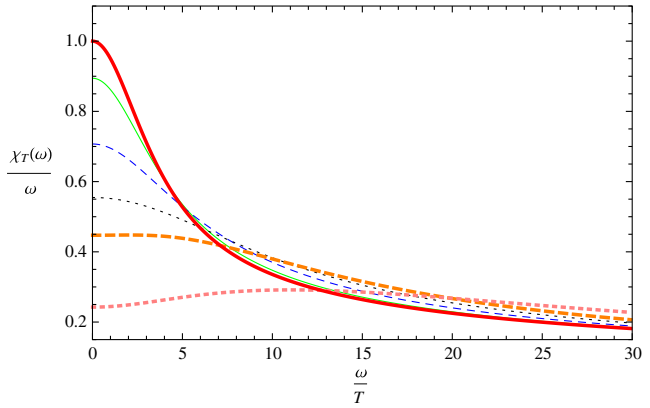


FIG. 1 (color online). D4/D6 model: trace of the spectral function for lightlike momenta divided by frequency, $\eta^{\mu\nu}\chi_{\mu\nu}(q=\omega)/\omega$, in units of $\mathcal{N}$, for the case $\vec{k} \parallel B$. Different curves correspond to different dimensionless magnetic fields: $\tilde{B}$=0 (red, thick solid), 0.5 (green, solid), 1.0 (blue, dashed), 1.5 (black, dotted), 2.0 (orange, thick dashed), and 4.0 (pink, thick dotted).

In the above equations, the dimensionless quantities $\{\tilde{\omega}, \tilde{q}, \tilde{B}\}$ are defined as in Eqs. (19) and (20). For the purpose of computing the retarded Green's function, which is related to the photon signals, this time we need the following on-shell action by integrating the action in Eq. (12) by parts:

$$S_{fl} = -\frac{\mathcal{N}'}{2}\int\frac{d^4k}{(2\pi)^4} \times\left\{\sqrt{-G}G^{uu}G^{yy}a_y(-k,u;B)\partial_u a_y(k,u;B) + \sqrt{-G}G^{uu}G^{zz}a_z(-k,u;B)\partial_u a_z(k,u;B)\right\}\Big|_{u=0}^{u=1}. \tag{32}$$

Then, the formulas for the retarded Green's function are the same as Eqs. (24) and (27), but with the modes $a_y(k,u;B)$ and $a_z(k,u;B)$ evolving according to Eqs. (30) and (31).

Although the longitudinal modes have no contribution to the photoemission rate, as mentioned above, they do contribute to the plasma conductivity and result in its anisotropic feature. Therefore, for later convenience we also list the equations of motion for vanishing spatial momentum, which are related to the plot of the ac conductivity. In the presence of the external magnetic field, the conductivity should be separated according to the direction with respect to the magnetic field:

$$\sigma_{xx}=\sigma_{yy}:\ \partial_u^2 a_x(k,u;B)+\left[\frac{f'(u)}{f(u)}-\frac{g'(u)}{2g(u)}\right]\partial_u a_x(k,u;B) + \frac{\tilde{\omega}^2}{uf(u)^2}a_x(k,u;B)=0, \tag{33}$$

$$\sigma_{zz}:\ \partial_u^2 a_z(k,u;B)+\left[\frac{f'(u)}{f(u)}+\frac{g'(u)}{2g(u)}\right]\partial_u a_z(k,u;B) + \frac{\tilde{\omega}^2}{uf(u)^2}a_z(k,u;B)=0. \tag{34}$$

We end this subsection by emphasizing that Eqs. (22), (30), and (31) are the main equations of motion as far as the electromagnetic signals are concerned. Explicitly, we see that due to the presence of the background magnetic field, which introduces anisotropy into the system, the gauge field behaves quite differently when changing the direction of its spatial momentum with respect to the direction of the magnetic field.

### C. Numerical results for the photoemission rate and conductivity

In Figs. 1 and 2 we plot the trace of the spectral function for the real photon production $\chi^{\mu}_{\mu}(q=\omega)/\omega$, weighted by a factor $\mathcal{N}$, for the cases $\vec{k} \parallel B$ and $\vec{k} \perp B$, respectively.

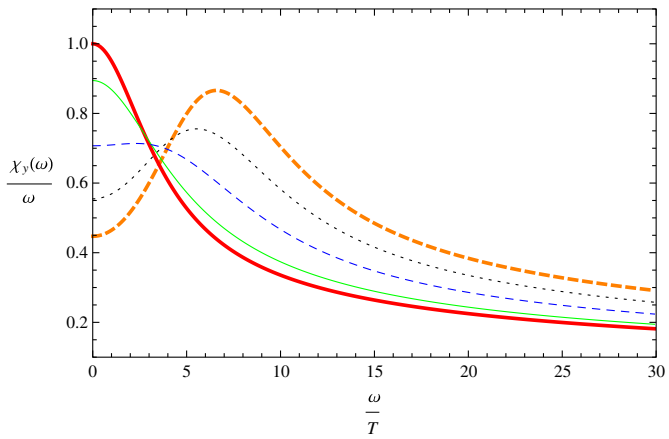


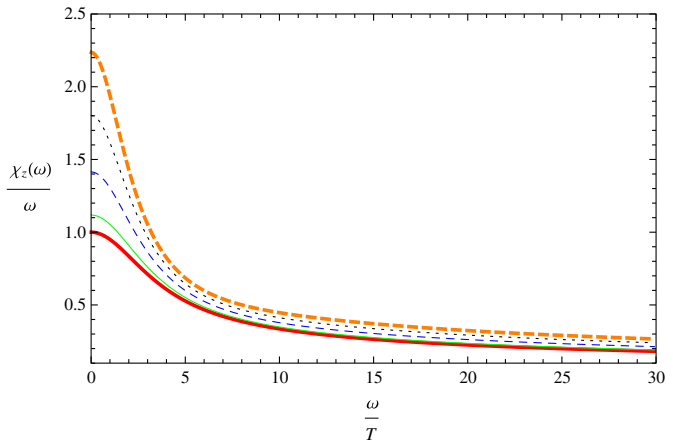


FIG. 2 (color online). D4/D6 model: trace of the spectral function for lightlike momenta divided by frequency, $\eta^{\mu\nu}\chi_{\mu\nu}(q=\omega)/\omega$, in units of $\mathcal{N}$, for the case $\vec{k} \perp B$. Different curves correspond to different dimensionless magnetic fields: $\tilde{B}$=0 (red, thick solid), 0.5 (green, solid), 1.0 (blue, dashed), 1.5 (black, dotted), and 2.0 (orange, thick dashed).

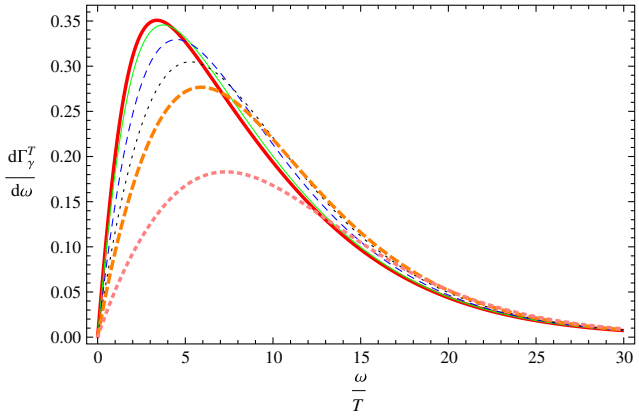


FIG. 3 (color online). D4/D6 model: photoproduction rate $d\Gamma_\gamma^T/d\omega$ (for the case $\vec{k} \parallel B$), weighted in units of $\mathcal{N}\frac{e^2}{4\pi}$, at different dimensionless magnetic fields corresponding to Fig. 1.

Concentrating on the $\tilde{B} = 0$ curve (the red line), we find that the trace of the spectral function $\chi_\mu^\mu(q = \omega)/\omega$ has a linear behavior in the large-frequency regime. An analytical computation of the spectral function in the low-/high-frequency regimes has been carried out in Refs. [7,9], which is consistent with our numerical result. Once the magnetic field is switched on, the linear regime in the trace spectral function narrows, which can also be read off from Figs. 3 and 4 for the photoemission rates. From the different curves in Fig. 1, we conclude that the magnetic field significantly weakens the spectral function in the low-$\omega/T$ regime for the case that produced photons move along the direction of the magnetic field. However, this is quite different from the conclusions obtained from Fig. 2 for the case $\vec{k} \perp B$: the right part of Fig. 2 shows that the presence of the magnetic field enlarges the spectral function in the infrared regime of the frequency. Moreover, we can see that in the left part of Fig. 2 there is a peak feature in the spectral function at nonzero frequency when the magnetic field is increased to a certain value (see the orange line).

Figures 3 and 4 are for the profiles of the photoemission rates $d\Gamma_\gamma/d\omega$, from the QCD-like plasma dual to the D4/D6 model, with $\vec{k} \parallel B$ and $\vec{k} \perp B$, respectively. These two figures constitute the main result of this paper. The anisotropic characteristic induced by the external magnetic field can be clearly read off from these plots. More specifically, when the produced photons move along the direction of the external magnetic field, the photoproduction rates become suppressed when increasing the magnetic field, as seen from Fig. 3. In sharp contrast to this, when the produced photons move along a direction perpendicular to the magnetic field, the magnetic field has the effect of amplifying the photoemission signal. Concentrating on the latter case, $\vec{k} \perp B$, we find that for $d\Gamma_\gamma^y/d\omega$ there is a blueshift for the peak frequency $\omega_p$, at which the photoproduction rate maximizes, while increasing the magnetic field. On the contrary, the peak frequency is redshifted in the plots for $d\Gamma_\gamma^T/d\omega$ and $d\Gamma_\gamma^z/d\omega$. The large-$\omega$ behavior is dominated by the suppression of the Bose-Einstein factor. However, the profiles for the photoproduction rate are quite different from that of the black-body radiation spectrum, especially in the intermediate regime of the frequency space. This is consistent with the claim of Ref. [7] that the photoproduction rate from the QCD plasma has nothing to do with the black-body radiation, and is not only due to the thermal effect.

In Figs. 5 and 6 we plot the ac conductivity of the QCD-like plasma dual to the D4/D6 model at different magnetic fields. From the conductivity profiles, we can obtain much information about the holographic plasma. Our analysis for the conductivity profiles will be concentrated on the infrared regime of the frequency $\omega$ as the effect of the magnetic field is washed out in the large-$\omega$ regime. We just mention one striking characteristic of the conductivity profiles. The magnetic field has quite a different effect on the value of the ac conductivity: the conductivity along the transverse direction (with respect to the direction of the magnetic

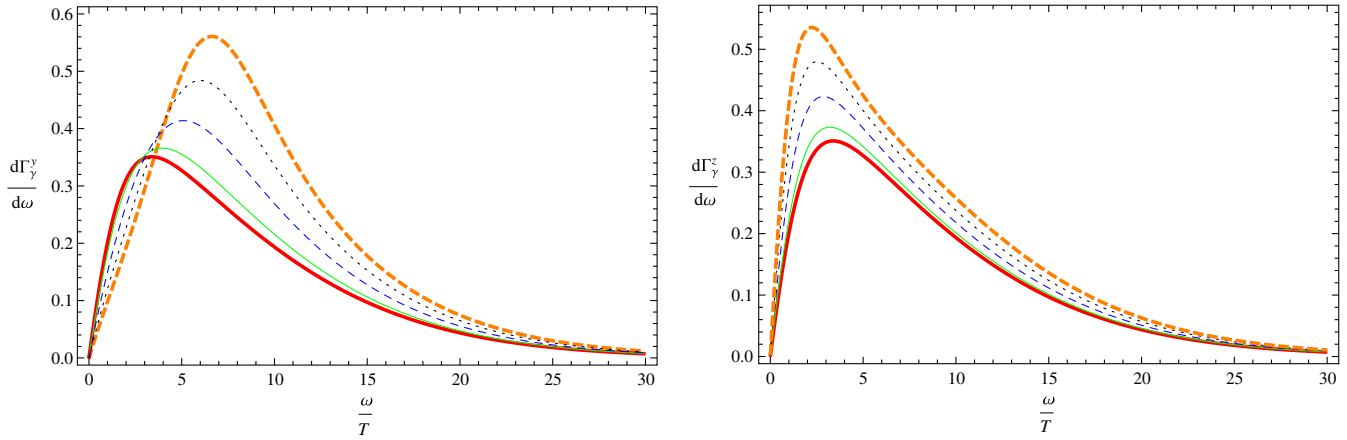


FIG. 4 (color online). D4/D6 model: photoproduction rates $d\Gamma_\gamma^y/d\omega$ and $d\Gamma_\gamma^z/d\omega$ (for the case $\vec{k} \perp B$), weighted in units of $\mathcal{N}\frac{e^2}{4\pi}$, at different dimensionless magnetic fields corresponding to Fig. 2.

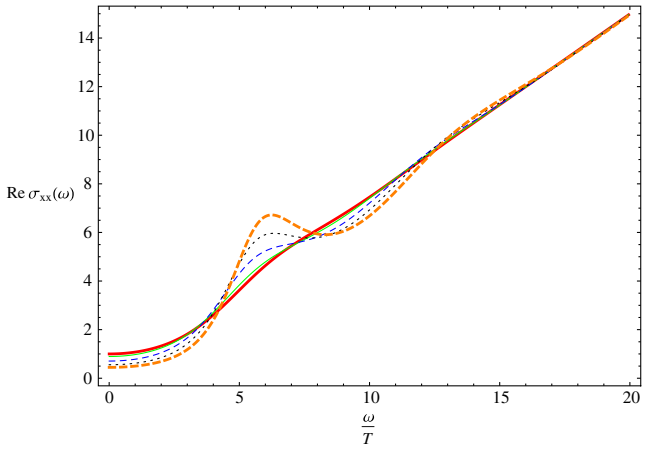


FIG. 5 (color online). D4/D6 model: real part of the ac conductivity along the $x$ direction at different magnetic fields corresponding to Fig. 2.

field) gets suppressed, and eventually a gap structure will appear at a certain value of $B$. This is consistent with the claim that a magnetic field can induce the gap formation; however, for the conductivity along the longitudinal direction, the magnetic field—just like the baryon density—increases the conducting ability of the QCD-like plasma; see for example Ref. [15] for more detailed discussions. This point also explicitly shows the anisotropic feature of the sQGP induced by the external magnetic field.

In Sec. IV, we will consider the D3/D7 model and carry out computations parallel to this section. We will find that the results obtained in this section are straightforwardly generalized to the D3/D7 model. These consistent results, obtained from the AdS/CFT approach, once again show some universal properties of the holographic plasma. To be optimistic, it is reasonable to believe that these studies—under the framework of toy models—can give us some hints for understanding some phenomena related to strong-coupling dynamics. Needless to say, there are some explicit defects in our studies. The first one is with regards to the massless limit for the flavor quark. Taking this limit greatly simplifies our numerical evaluations as well as the analytical derivation of the equations of motion. However, the vector and scalar modes will mix together once they go beyond the massless limit. To overcome this problem, some careful treatments for the operator mixing under the holographic framework have been proposed in Ref. [29]. In these works, the authors interpreted the operator mixing as the holographic renormalization-group flow.

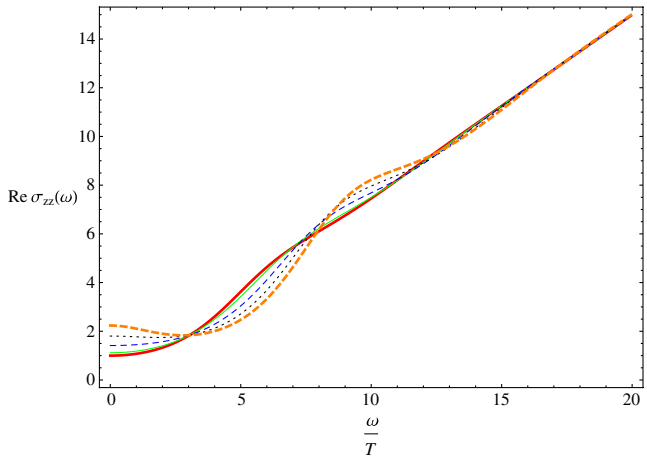


FIG. 6 (color online). D4/D6 model: real part of the ac conductivity along the $z$ direction corresponding to different magnetic fields as in Fig. 5.

## IV. D3/D7 SYSTEM

### A. Main equations

The other intersecting D-brane system considered in this paper is the better-studied D3/D7 model. In this subsection, we list the main equations of motion, which are the starting points for numerically computing the photoemission rate and plasma conductivity in this brane model. The numerical results will be presented in Sec. IV B as several figures.

The supergravity geometry for many coincident D3-brane is

$$ds^2 = \left(\frac{u_0}{R}\right)^2 \frac{1}{u^2}(-f(u)dt^2 + d\vec{x}^2) + \left(\frac{R}{u}\right)^2 \frac{du^2}{f(u)} + R^2 d\Omega_5^2, \tag{35}$$

where the internal space $\Omega_5$ is parametrized as

$$d\Omega_5^2 = d\theta^2 + \sin^2\theta d\xi^2 + \cos^2\theta d\Omega_3^2, \tag{36}$$

and

$$e^{\phi} = \text{constant}, \qquad f(u) = 1 - u^4, \qquad T = \frac{u_0}{\pi R^2}. \tag{37}$$

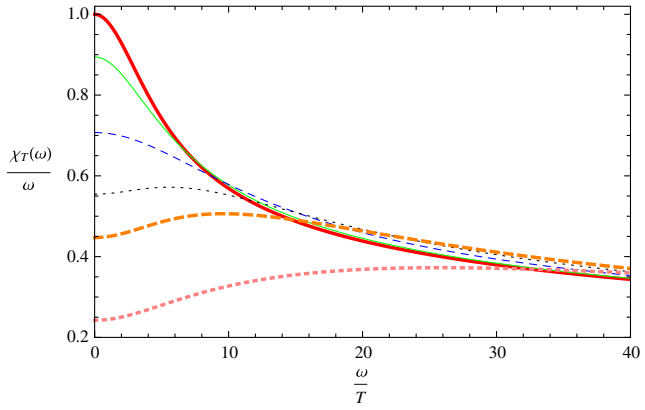


FIG. 7 (color online). D3/D7 model: trace of the spectral function for lightlike momenta divided by frequency, $\eta^{\mu\nu}\chi_{\mu\nu}(q = \omega)/\omega$, in units of $\mathcal{N}$, for the case $\vec{k} \parallel B$. Different curves correspond to different dimensionless magnetic fields as in Fig. 1.

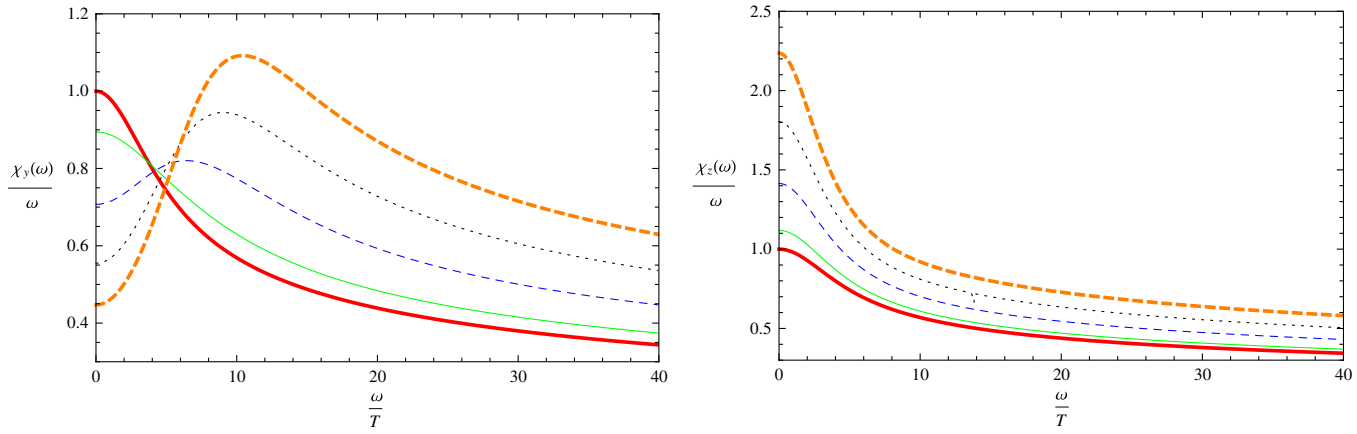


FIG. 8 (color online). D3/D7 model: trace of the spectral function for lightlike momenta divided by frequency, $\eta^{\mu\nu}\chi_{\mu\nu}(q=\omega)/\omega$, in units of $\mathcal{N}$, for the case $\vec{k} \perp B$. Different curves correspond to different dimensionless magnetic fields as in Fig. 2.

As in the D4/D6 system, the quark sector can be introduced in the quenched approximation by adding a probe D7-brane into the above black hole geometry. The flavor D7-brane extends along $(t, \vec{x}, u, \Omega_3)$ and its embedding profile is encoded in the function $\theta(u)$. However, in this paper we mainly consider the chiral-symmetry-restoring phase and the massless limit for the flavor quark, which amounts to saying that the embedding profile for the flavor brane is trivial. Therefore the induced metric on the world-volume of the flavor D7-brane is Schwarzschild-AdS$_5 \times S^3$:

$$ds^2 = \left(\frac{u_0}{R}\right)^2 \frac{1}{u^2}(-f(u)dt^2 + d\vec{x}^2) + \left(\frac{R}{u}\right)^2 \frac{du^2}{f(u)} + R^2 d\Omega_3^2. \tag{38}$$

We now directly list the equations of motion for the flavor U(1) sector, as the details are in parallel with those of Sec. III. As mentioned in Sec. III, due to the presence of the magnetic field, the SO(3) rotational symmetry is partially broken and we have to treat the cases $\vec{k} \parallel B$ and $\vec{k} \perp B$ separately. Furthermore, in both cases the longitudinal modes have no contributions to the photon signal, as mentioned in Sec. III A. In what follows we only write down the equations for the transverse modes for conciseness. First consider the $\vec{k} \parallel B$ case, where there are two identical transverse modes $a_x$ and $a_y$, which obey the following equation of motion:

$$\partial_u^2 a_{x(y)}(k,u;B) + \left[\frac{f'(u)}{f(u)} - \frac{1}{u} - \frac{g'(u)}{2g(u)}\right]\partial_u a_{x(y)}(k,u;B) + \left[\frac{\tilde{\omega}^2}{f(u)^2} - \frac{\tilde{q}^2}{f(u)}\right]a_{x(y)}(k,u;B) = 0, \tag{39}$$

where the dimensionless frequency $\tilde{\omega}$ and momentum $\tilde{q}$ are defined as

$$\tilde{\omega} = \frac{\omega}{4\pi T}, \qquad \tilde{q} = \frac{q}{4\pi T},$$

and the function $g(u)$ is given by

$$g(u) = 1 + \tilde{B}^2 u^4, \qquad \tilde{B} = \left(\frac{R}{u_0}\right)^2 B.$$

The next step is to consider the $\vec{k} \perp B$ case. This case is more complex, as now there are two different transverse modes $a_y$ and $a_z$:

$$\partial_u^2 a_y(k,u;B) + \left[\frac{f'(u)}{f(u)} - \frac{1}{u} - \frac{g'(u)}{2g(u)}\right]\partial_u a_y(k,u;B) + \left[\frac{\tilde{\omega}^2}{f(u)^2} - \frac{\tilde{q}^2}{f(u)g(u)}\right]a_y(k,u;B) = 0, \tag{40}$$

$$\partial_u^2 a_z(k,u;B) + \left[\frac{f'(u)}{f(u)} - \frac{1}{u} + \frac{g'(u)}{2g(u)}\right]\partial_u a_z(k,u;B) + \left[\frac{\tilde{\omega}^2}{f(u)^2} - \frac{\tilde{q}^2}{f(u)g(u)}\right]a_z(k,u;B) = 0. \tag{41}$$

For completeness, we also list the equations of motion in the case of $\vec{k} = 0$, which are related to the evaluation of the

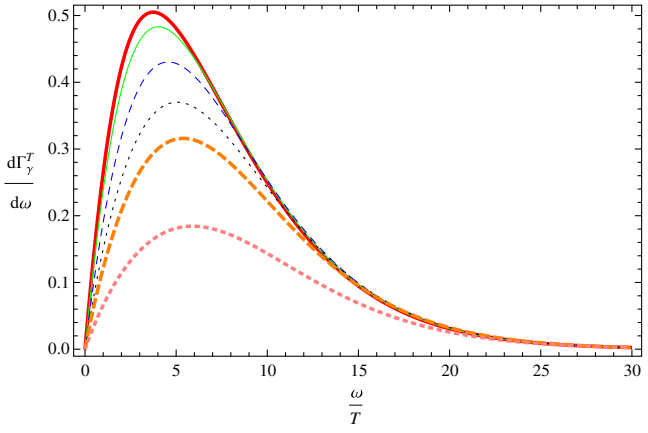


FIG. 9 (color online). D3/D7 model: photoproduction rate $d\Gamma_\gamma^T/d\omega$ (for the case $\vec{k} \parallel B$), weighted in units of $\mathcal{N}\frac{e^2}{4\pi}$, at different dimensionless magnetic fields corresponding to Fig. 1.

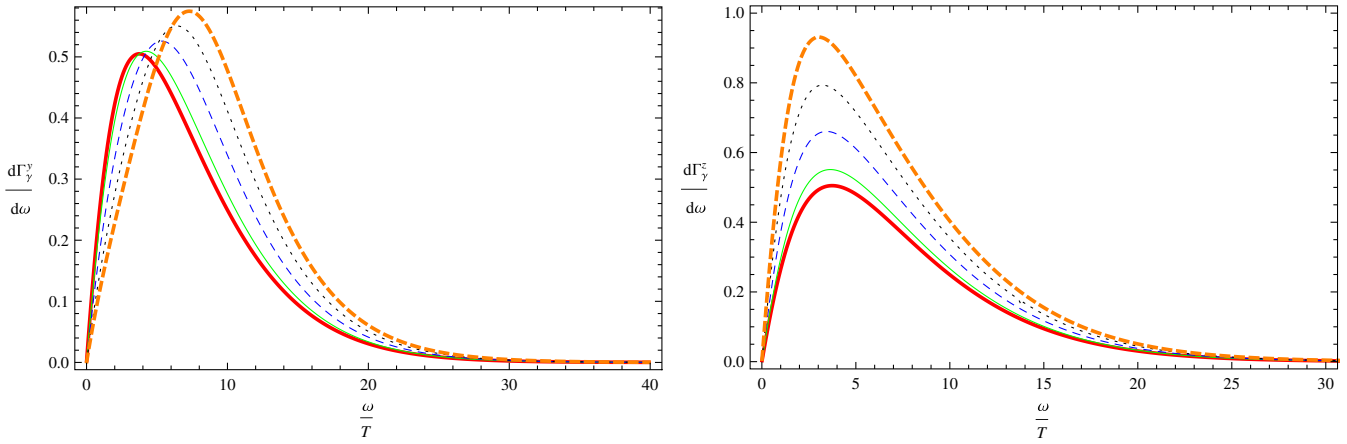


FIG. 10 (color online). D3/D7 model: photoproduction rates $d\Gamma_\gamma^y/d\omega$ and $d\Gamma_\gamma^z/d\omega$ (for the case $\vec{k} \perp B$), weighted in units of $\mathcal{N}\frac{e^2}{4\pi}$, at different dimensionless magnetic field corresponding to Fig. 2.

plasma conductivity. As in the D4/D6 model, the conductivities should be separated according to their direction with respect to the magnetic field:

$$\sigma_{xx} = \sigma_{yy}: \partial_u^2 a_x(k,u;B) + \left[\frac{f'(u)}{f(u)} - \frac{1}{u} - \frac{g'(u)}{2g(u)}\right]\partial_u a_x(k,u;B) + \frac{\tilde{\omega}^2}{f(u)^2} a_x(k,u;B) = 0, \tag{42}$$

$$\sigma_{zz}: \partial_u^2 a_z(k,u;B) + \left[\frac{f'(u)}{f(u)} - \frac{1}{u} + \frac{g'(u)}{2g(u)}\right]\partial_u a_z(k,u;B) + \frac{\tilde{\omega}^2}{f(u)^2} a_z(k,u;B) = 0. \tag{43}$$

### B. Numerical results for the photoemission and conductivity

In what follows, we present our numerical results in several figures. In Figs. 7 and 8, we plot the trace of the spectral function for lightlike momenta, $\chi_\mu^\mu(q=\omega)/\omega$. Figures 9 and 10 are for the plot of the photoemission rate $d\Gamma/d\omega$ from the QCD-like plasma. In the last two figures, Figs. 11 and 12, we plot the real parts of the ac conductivity of the dense holographic plasma described by the D3/D7 model.

As in the D4/D6 system, due to the presence of the magnetic field we have to treat the photon signals (embedded in the plots of the spectral function and photoemission rate) separately. As mentioned at the end of Sec. III, the associated results presented in this subsection are basically the same as those of the D4/D6 model. Before closing this section, we give the explicit form of the prefactor $\mathcal{N}$, which roughly measures the degrees of freedom for the quark-gluon plasma:

$$\mathcal{N} = \gamma N_f N_c T^2,$$

with $N_f$ and $N_c$ counting the number of the color-brane (D3- or D4-brane) and the flavor-brane (D6- or D7-brane). The model dependent factor $\gamma$ is

$$\gamma = \begin{cases} \frac{1}{9\pi^2}, & \text{D4/D6 model,} \\ \frac{1}{2\pi}, & \text{D3/D7 model.} \end{cases}$$

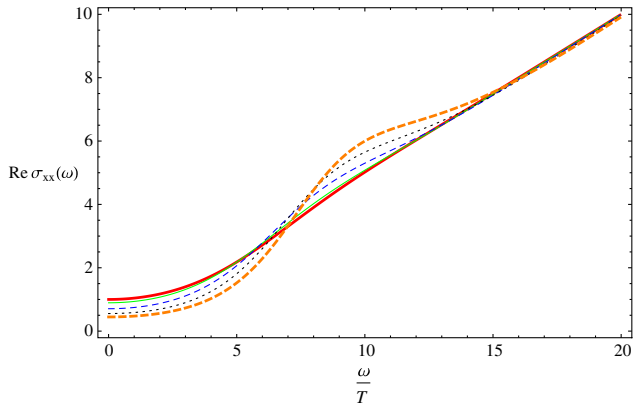


FIG. 11 (color online). D3/D7 model: real part of the ac conductivity along the $x$ direction at different magnetic fields as in Fig. 2.

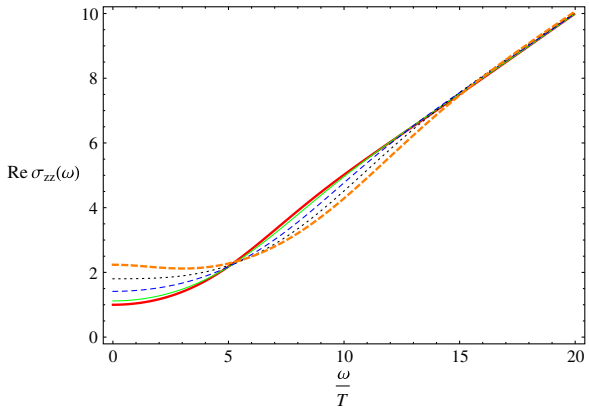


FIG. 12 (color online). D3/D7 model: real part of the ac conductivity along the $z$ direction at different magnetic fields as in Fig. 2.

## V. SUMMARY AND DISCUSSION

In this paper we used two holographic QCD models to study one important signal of the sQGP, i.e., the photoemission rate from the QCD-like plasma at finite magnetic field. One important finding of our study is that the magnetic field can induce the anisotropic feature in the photon signal from the QCD-like plasma, which is consistent with the proposal [23] that the observed anisotropic feature of the quark-gluon plasma—produced in heavy-ion experiments—can be understood as the effect of a large magnetic field. More explicitly, we see that when the produced photons are moving along the magnetic field, the photon signal is weakened as the magnetic field increases; on the other hand, when the produced photons move perpendicular to the magnetic field, the magnetic field has the effect of amplifying the electromagnetic signature. However, in our analysis we do not consider a very large magnetic field, which is reflected in theprobe limit for the flavor brane. One naive idea towards studying the electromagnetic signatures from quark-gluon plasma at large magnetic field is to consider the magnetically charged black hole in AdS spacetime. We leave this for future work. Another feature induced by the magnetic field is the ac conductivity of the holographic plasma. As is seen in this paper, the magnetic field does have the effect of generating a pseudogap structure in the conductivity along the direction perpendicular to the magnetic field.

## ACKNOWLEDGMENTS

The author would like to thank Johanna Erdmenger for her encouragement and inspirations as well as for some good suggestions during this project. This work was supported by the MPS-CAS Doctoral Training program.

[1] E. Shuryak, Prog. Part. Nucl. Phys. **53**, 273 (2004); E. Shuryak, arXiv:hep-ph/0608177.
[2] J. M. Maldacena, Adv. Theor. Math. Phys. **2**, 231 (1998).
[3] J. Erdmenger, N. Evans, I. Kirsch, and E. Threlfall, Eur. Phys. J. A **35**, 81 (2008); R. Myers and S. Vazquez, Classical Quantum Gravity **25**, 114008 (2008); E. Iancu, Acta Phys. Pol. B **39**, 3213 (2008); S. S. Gubser and A. Karch, Annu. Rev. Nucl. Part. Sci. **59**, 145 (2009); U. Gursoy, Mod. Phys. Lett. A **23**, 3349 (2008); R. A. Janik, Lect. Notes Phys. **828**, 147 (2011); J. Casalderrey-Solana, H. Liu, D. Mateos, K. Rajagopal, and U. A. Wiedemann, arXiv:1101.0618; A. Karch, AIP Conf. Proc. **1441**, 95 (2012).
[4] M. Kruczenski, D. Mateos, R. C. Myers, and D. J. Winters, J. High Energy Phys. 05 (2004) 041; T. Sakai and S. Sugimoto, Prog. Theor. Phys. **113**, 843 (2005); J. Erlich, E. Katz, D. T. Son, and M. A. Stephanov, Phys. Rev. Lett. **95**, 261602 (2005); L. Da Rold and A. Pomarol, Nucl. Phys. **B721**, 79 (2005).
[5] A. Karch, E. Katz, D. T. Son, and M. A. Stephanov, Phys. Rev. D **74**, 015005 (2006).
[6] U. Gursoy and E. Kiritsis, J. High Energy Phys. 02 (2008) 032; U. Gursoy, E. Kiritsis, and F. Nitti, J. High Energy Phys. 02 (2008) 019.
[7] S. Caron-Huot, P. Kovtun, G. D. Moore, A. Starinets, and L. G. Yaffe, J. High Energy Phys. 12 (2006) 015.
[8] D. Mateos and L. Patino, J. High Energy Phys. 11 (2007) 025.
[9] A. Parnachev and D. A. Sahakyan, Nucl. Phys. **B768**, 177 (2007).
[10] A. N. Atmaja and K. Schalm, J. High Energy Phys. 08 (2010) 124.
[11] A. Rebhan and D. Steineder, J. High Energy Phys. 08 (2011) 153.
[12] B. Hassanain and M. Schvellinger, Phys. Rev. D **85**, 086007 (2012).
[13] J. Mas, J. P. Shock, J. Tarrio, and D. Zoakos, J. High Energy Phys. 09 (2008) 009.
[14] K. Jo and S.-J. Sin, Phys. Rev. D **83**, 026004 (2011).
[15] Y. Y. Bu, Phys. Rev. D **86**, 026003 (2012).
[16] Y.-Y. Bu and J. M. Yang, Nucl. Phys. **B855**, 388 (2012).
[17] Y. Y. Bu and J. M. Yang, Phys. Rev. D **84**, 106004 (2011).
[18] Y.-Y. Bu, Nucl. Phys. **B864**, 806 (2012).
[19] V. G. Filev, C. V. Johnson, R. Rashkov, and K. Viswanathan, J. High Energy Phys. 10 (2007) 019.
[20] T. Albash, V. G. Filev, C. V. Johnson, and A. Kundu, J. High Energy Phys. 07 (2008) 080.
[21] J. Erdmenger, R. Meyer, and J. P. Shock, J. High Energy Phys. 12 (2007) 091.
[22] A. Adare *et al.* (PHENIX Collaboration), Phys. Rev. Lett. **109**, 122302 (2012).
[23] G. Basar, D. Kharzeev, D. Kharzeev, and V. Skokov, Phys. Rev. Lett. **109**, 202303 (2012).
[24] D. E. Kharzeev, L. D. McLerran, and H. J. Warringa, Nucl. Phys. **A803**, 227 (2008).
[25] M. L. Bellac, *Thermal field theory* (Cambridge University Press, Cambridge, England, 1996).
[26] P. K. Kovtun and A. O. Starinets, Phys. Rev. D **72**, 086009 (2005).
[27] D. T. Son and A. O. Starinets, J. High Energy Phys. 09 (2002) 042.
[28] A. Karch and E. Katz, J. High Energy Phys. 06 (2002) 043.
[29] I. Amado, M. Kaminski, and K. Landsteiner, J. High Energy Phys. 05 (2009) 021; M. Kaminski, K. Landsteiner, J. Mas, J. P. Shock, and J. Tarrio, J. High Energy Phys. 02 (2010) 021.